J. Automation & Systems Engineering 12-4 (2018): 1-13

Regular paper

Stability Analysis of Sliding Mode and Backstepping in Dual Stator Winding Induction Machine Control

Noureddine Layadi [1], A. Djerioui [1], S. Zeghlache [2], A. Houari [3], M. F. Benkhoris [3] and F. Berrabah [1]

[1] Laboratoire de Génie Electrique, Department of Electrical Engineering Faculty of technology, University Mohamed Boudiaf of M'Sila, BP 166, Ichbilia, M'Sila, 28000, Algeria
(layadinoureddine1@gmail.com, alidjerioui@yahoo.fr, Fouadberrabah1@gmail.com)

[2] Laboratoire d'Analyse des Signaux et Systèmes, Department of Electronics, Faculty of technology, University Mohamed Boudiaf of M'Sila, BP 166, Ichbilia, M'Sila, 28000, Algeria
(zegsam5@gmail.com)

[3] IREENA Laboratory, University of Nantes, Saint-Nazaire, France
(Azeddine.Houari@univ-nantes.fr, Mohamed-Fouad.Benkhoris@univ-nantes.fr)

JASE
Journal of Automation & Systems Engineering

Abstract-This paper presents a stability study of a dual stator winding Induction Machine (DSWIM) using two methods of nonlinear control: sliding mode control (SMC) and backstepping control (BSC). The DSWIM is powered by two three-phase voltage source inverters (VSI) with two levels using a pulse width modulation (PWM) control strategy. The simulation results using Matlab/Simulink show the performance of each controller when the machine is operating in a healthy state and under parametric variation, indicators performance prove that the BSC has a slight superiority in term of stability performance compared to SMC in steady state.

Keywords: Dual stator winding induction machine, Backstepping control, Sliding mode control, Stability, Robustness.

Article history: Received 04 August 2018, Accepted 25 December 2018

1. INTRODUCTION

The dual stator winding induction machine (DSWIM) belongs to the category of multiphase machines. It has been proposed for different fields of the industry that need high power, such as hybrid electric vehicles, locomotive traction and ship propulsion. DSWIM not only guarantees a decrease of rotor harmonics currents and torque pulsations, but also offers many other advantages, such as: reliability, power segmentation and higher efficiency [1, 2].

Backstepping control (BSC) is able to effectively linearize a non-linear system [3]. BSC not only guarantees high performance in both dynamic and steady state, it also provides excellent closed-loop stability and good tracking, even in the event of an open-phase fault [1]. The only disadvantage of BSC is the setting of gains.

Sliding mode control (SMC) is a non-linear control. It has a fast dynamic response where system stability is guaranteed by reducing transient state errors. The SMC ensures robustness against parameter variations and external disturbances when the system reaches and stays on the sliding surface. On the other hand, the SMC has a disadvantage called chatter. This undesirable phenomenon is in the form of high frequency ripples caused by the switching control law. SMC has recently been applied to a doubly fed induction generator, where it has proven robust against parameter variations and disturbances in front of the backstepping control [4].

This paper presents comparative studies between sliding mode control and backstepping control of DSWIM in healthy operation and under parametric variation accompanied by simulation results and a stability analysis to show the efficiency and robustness of each control method.

This paper is organized as follows: In section 2, the dynamic model of the DSWIM is given. In section 3, the SMC is designed. The BSC is developed in section 4. Simulation results are shown and analyzed in section 5. Finally, the conclusion is given in section 6.

2. DSWIM MODELLING

The d-q dynamic healthy model of the squirrel cage dual stator winding Induction Machine with a reference frame fixed to the rotor is given by:

$$\begin{cases} \frac{d}{dt} i_{sd1} = \frac{1}{L_{s1}} \left[v_{sd1} - R_{s1} i_{sd1} + \omega_s \left(L_{s1} i_{sq1} + T_r \varphi_r \omega_{gl} \right) \right] \\ \frac{d}{dt} i_{sq1} = \frac{1}{L_{s1}} \left[v_{sq1} - R_{s1} i_{sq1} - \omega_s \left(L_{s1} i_{sd1} + \varphi_r \right) \right] \\ \frac{d}{dt} i_{sd2} = \frac{1}{L_{s2}} \left[v_{sd2} - R_{s2} i_{sd2} + \omega_s \left(L_{s2} i_{sq2} + T_r \varphi_r \omega_{gl} \right) \right] \\ \frac{d}{dt} i_{sq2} = \frac{1}{L_{s2}} \left[v_{sq2} - R_{s2} i_{sq2} - \omega_s \left(L_{s2} i_{sd2} + \varphi_r \right) \right] \\ \frac{d}{dt} \omega_r = \frac{1}{J} \left[p^2 \frac{L_m}{L_m + L_r} \varphi_r \left(i_{sq1} + i_{sq2} \right) - p T_L - K_f \omega_r \right] \\ \frac{d}{dt} \varphi_r = -\frac{R_r}{L_m + L_r} \varphi_r + \frac{L_m R_r}{L_m + L_r} \left(i_{sd1} + i_{sd2} \right) \end{cases} \quad (1)$$

Where: v_{sd1}, v_{sq1} are stator1 voltages components. v_{sd2}, v_{sq2} are stator2 voltages components. i_{sd1}, i_{sq1} are stator1 currents components. i_{sd2}, i_{sq2} are stator2 currents components. L_{s1}, L_{s2}, L_r and L_m are stator1, stator2, rotor and mutual inductance, respectively. R_{s1}, R_{s2} and R_r are respectively stator1, stator2 and rotor resistance. $T_r = L_r / R_r$ is the rotor time constant. T_L is the applied load torque. ω_r is the rotor speed. J, K_f denote the rotor inertia and friction coefficient. ω_s is the stator pulsation. ω_{gl} is the slip pulsation. φ_r is the rotor flux. p denotes the number of pole pairs. The subscripts d, q designate direct and quadrate indices according to the usual d-q axis components in the synchronous rotating frame.

3. SLIDING MODE CONTROL

3.1 Sliding mode theory

Sliding mode control is based on the convergence of system state trajectory to a sliding surface. The state vector is kept around this surface by the switching control effort so that the trajectory slides to the origin through the sliding surface. The design of SMC can be achieved in two successive steps [5]:

- **First step**: definition of sliding surfaces

The most used surface S(x) in the literature is given by:

$$S(t) = \left(\lambda + \frac{d}{dt}\right)^{r-1} (x_{ref} - x) \tag{2}$$

Where: x is the state vector, x_{ref} is the reference state vector, r is the degree of the sliding mode and λ is the weighting factor.

- **Second step**: Control law design

The sliding mode control has two command components and can be written as follows:

$$u(t) = u_{eq}(t) + u_N(t) \tag{3}$$

The component u_{eq} called the equivalent control (decoupling control) is obtained by putting surface derivate equals zero $\dot{S}(t) = 0$, its role is holding the system on the sliding surface that is defined by $S(t) = 0$. The other constituent u_N is the discontinuous control (switching control) which ensures the convergence of system state trajectory toward sliding surface. The reaching condition is based on Lyapunov theory stability and must verify $\dot{S}.S < 0$.

3.2 Application of SMC on DSWIM

The SMC algorithm for DSWIM has been presented in [6]. In order to eliminate or decrease the chattering phenomena in steady state, a saturation function sat(t) is used instead of the "signum" function (sgn(t)) for the switching control. The sat(t) function is defined as follows:

$$sat(S) = \frac{S}{|S| + m} \tag{4}$$

Where: m is a small positive gain and $|S| >> m$. Therefore, the SMC for DSWIM can be designed as follows:

- **Speed and flux SMC:**

Speed and flux surface:

$$\begin{cases} S(\omega_r) = \omega_r^* - \omega_r \\ S(\varphi_r) = \varphi_r^* - \varphi_r \end{cases} \tag{5}$$

The time derivative of (5) gives:

$$\begin{cases} \dot{S}(\omega_r) = \dot{\omega}_r^* - \dot{\omega}_r \\ \dot{S}(\varphi_r) = \dot{\varphi}_r^* - \dot{\varphi}_r \end{cases} \tag{6}$$

Where: ω_r^* and φ_r^* are the reference of speed and flux, respectively. By substituting (1) into (6) we obtain:

$$\begin{cases} \dot{S}(\omega_r) = \dot{\omega}_r^* - \dfrac{p^2}{J}\dfrac{L_m}{L_m + L_r}(i_{sq1} + i_{sq2})\varphi_r - \dfrac{K_f}{J}\omega_r - \dfrac{p}{J}T_L \\ \dot{S}(\varphi_r) = \dot{\varphi}_r^* + \dfrac{R_r}{L_m + L_r}\varphi_r - \dfrac{L_m R_r}{L_m + L_r}(i_{sd1} + i_{sd2}) \end{cases} \tag{7}$$

Putting:

$$\begin{cases} i_{sq1} + i_{sq2} = i_{sq}^* = i_{sqeq} + i_{sqn} \\ i_{sd1} + i_{sd2} = i_{sd}^* = i_{sdeq} + i_{sdn} \end{cases} \tag{8}$$

Where: i_{sq}^* and i_{sd}^* are the reference currents.

Assuming that:

$$\begin{cases} i_{sd1}^* = i_{sd1}^* = \dfrac{i_{sd}^*}{2} \\ i_{sq1}^* = i_{sq2}^* = \dfrac{i_{sq}^*}{2} \end{cases} \tag{9}$$

Using (7) and (8), we obtain:

$$\begin{cases} \dot{S}(\omega_r) = \dot{\omega}_r^* - \dfrac{p^2}{J}\dfrac{L_m}{L_m + L_r}\varphi_r(i_{sqeq} - i_{sqn}) + \dfrac{K_f}{J}\omega_r + \dfrac{p}{J}T_L \\ \dot{S}(\varphi_r) = \dot{\varphi}_r^* + \dfrac{R_r}{L_m + L_r}\varphi_r - \dfrac{L_m R_r}{L_m + L_r}(i_{sdeq} + i_{sdn}) \end{cases} \tag{10}$$

Applying the SMC theory, we find the d-q axis components of currents control:

$$\begin{cases} i_{sdeq} = \dfrac{L_m + L_r}{R_r L_m}\left[\varphi_r^* + \dfrac{R_r}{L_m + L_r}\varphi_r\right] \\ i_{sqeq} = \dfrac{J}{p^2}\dfrac{L_m + L_r}{L_m}\varphi_r\left[\dot{\omega}_r^* + \dfrac{K_f}{J}\omega_r + \dfrac{p}{J}T_L\right] \\ i_{sqn} = k_\omega sat[S(\omega_r)] \\ i_{sdn} = k_\varphi sat[S(\varphi_r)] \end{cases} \tag{11}$$

Where k_φ and k_ω are positive constants

- **Currents SMC:**

Currents surface

$$\begin{cases} s(i_{sd1}) = i_{sd1}^{*} - i_{sd1} \\ s(i_{sq1}) = i_{sq1}^{*} - i_{sq1} \\ s(i_{sd2}) = i_{sd2}^{*} - i_{sd2} \\ s(i_{sq2}) = i_{sq2}^{*} - i_{sq2} \end{cases} \tag{12}$$

The derivative of (12) as a function of time is:

$$\begin{cases} \dot{S}(i_{sdi}) = \dfrac{d}{dt} i_{sdi}^{*} - \dfrac{d}{dt} i_{sdi} \qquad i = \overline{1,2} \\ \dot{S}(i_{sqi}) = \dfrac{d}{dt} i_{sqi}^{*} - \dfrac{d}{dt} i_{sqi} \qquad i = \overline{1,2} \end{cases} \tag{13}$$

Using (1), (13) becomes:

$$\begin{cases} \dot{S}\left(\dfrac{d}{dt} i_{sd1}\right) = \dfrac{d}{dt} i_{sd1}^{*} - \dfrac{1}{L_{s1}} \left[v_{sd1} - R_{s1} i_{sd1} + \omega_s \left(L_{s1} i_{sq1} + T_r \varphi_r \omega_{gl} \right) \right] \\ \dot{S}\left(\dfrac{d}{dt} i_{sq1}\right) = \dfrac{d}{dt} i_{sq1}^{*} - \dfrac{1}{L_{s1}} \left[v_{sq1} - R_{s1} i_{sq1} - \omega_s \left(L_{s1} i_{sd1} + \varphi_r \right) \right] \\ \dot{S}\left(\dfrac{d}{dt} i_{sd2}\right) = \dfrac{d}{dt} i_{sd2}^{*} - \dfrac{1}{L_{s2}} \left[v_{sd2} - R_{s2} i_{sd2} + \omega_s \left(L_{s2} i_{sq2} + T_r \varphi_r \omega_{gl} \right) \right] \\ \dot{S}\left(\dfrac{d}{dt} i_{sq2}\right) = \dfrac{d}{dt} i_{sq2}^{*} - \dfrac{1}{L_{s2}} \left[v_{sq2} - R_{s2} i_{sq2} - \omega_s \left(L_{s2} i_{sd2} + \varphi_r \right) \right] \end{cases} \tag{14}$$

Putting:

$$\begin{cases} v_{sd1} = v_{sd1}^{*} = v_{sd1eq} + v_{sd1n} \\ v_{sq1} = v_{sq1}^{*} = v_{sq1eq} + v_{sq1n} \\ v_{sd2} = v_{sd2}^{*} = v_{sd2eq} + v_{sd2n} \\ v_{sq2} = v_{sq2}^{*} = v_{sq2eq} + v_{sq2n} \end{cases} \tag{15}$$

Finally, following the same method used in the previous step, we obtain the decoupling control voltages:

$$\begin{cases} v_{sd1eq} = L_{s1} \dfrac{d}{dt} i_{sd1}^{*} + R_{s1} i_{sd1} - \omega_s \left(L_{s1} i_{sq1} + T_r \varphi_r \omega_{gl} \right) \\ v_{sq1eq} = L_{s1} \dfrac{d}{dt} i_{sq1}^{*} + R_{s1} i_{sq1} + \omega_s \left(L_{s1} i_{sd1} + \varphi_r \right) \\ v_{sd2eq} = L_{s2} \dfrac{d}{dt} i_{sd2}^{*} + R_{s2} i_{sd2} - \omega_s \left(L_{s2} i_{sq2} + T_r \varphi_r \omega_{gl} \right) \\ v_{sq2eq} = L_{s2} \dfrac{d}{dt} i_{sq2}^{*} + R_{s2} i_{sq2} + \omega_s \left(L_{s2} i_{sd2} + \varphi_r \right) \end{cases} \tag{16}$$

And, therefore, switching control voltages:

$$\begin{cases} v_{sd1n} = k_{sd1} sat\left[S\left(i_{sd1}\right)\right] \\ v_{sq1n} = k_{sq1} sat\left[S\left(i_{sq1}\right)\right] \\ v_{sd2n} = k_{sd2} sat\left[S\left(i_{sd2}\right)\right] \\ v_{sq2n} = k_{sq2} sat\left[S\left(i_{sq2}\right)\right] \end{cases} \tag{17}$$

Where: k_{sd1}, k_{sq1}, k_{sd2} and k_{sq2} are positive gains that stabilize the closed-loop system and are obtained by adjustment.

4. BACKSTEPPING CONTROL

BSC establishes the global law of control in several steps. The intermediate command (virtual command) provided by each subsystem serves as a reference signal for the next step until the completion of the control design (actual control), where the global Lyapunov function associated is the sum of all the Lyapunov functions adapted to each backstepping stage, the BSC design for DSWIM is developed in two consecutive steps according to the backstepping algorithm presented in [7].

4.1 Step1: Flux and speed control (virtual control)

This step forces the rotor flux φ_r and the speed ω_r to reach their desired references φ_r^* and ω_r^*, respectively by identifying their errors Z_1 and Z_2, which means finding the virtual control guaranteeing this convergence. Flux and speed tracking errors are given by:

$$\begin{cases} Z_1 = \omega_r^* - \omega_r \\ Z_2 = \varphi_r^* - \varphi_r \end{cases} \tag{18}$$

The derivative of (18) gives:

$$\begin{cases} \dot{Z}_1 = \dot{\omega}_r^* - \dot{\omega}_r \\ \dot{Z}_2 = \dot{\varphi}_r^* - \dot{\varphi}_r \end{cases} \tag{19}$$

Using (1), (19) becomes:

$$\begin{cases} \dot{Z}_1 = \dot{\omega}_r^* - \dfrac{p^2}{J}\dfrac{L_m}{L_m + L_r}\varphi_r\left(i_{sq1} + i_{sq2}\right) + T_L\dfrac{p}{J} + \dfrac{K_f}{J}\omega_r \\ \dot{Z}_2 = \varphi_r^* + \dfrac{R_r}{L_m + L_r}\varphi_r - \dfrac{R_r L_m}{L_m + L_r}(i_{sd1} + i_{sd2}) \end{cases} \tag{20}$$

The first Lyapunov function candidate adapted to rotor flux and speed errors is defined by:

$$V_1 = \frac{1}{2}\left(Z_1^2 + Z_2^2\right) \tag{21}$$

The time derivative of (21) is:

$$\dot{V}_1 = Z_1\dot{Z}_1 + Z_2\dot{Z}_2 \tag{22}$$

To achieve stability according to the Lyapunov theory, the derivate of V_1 must be negative definite, in this case, we take:

$$\dot{Z}_1 = -K_i Z_i \qquad i = \overline{1,2} \tag{23}$$

Replacing (23) into (22), the derivate of the first Lyapunov function becomes:

$$\dot{V}_1 = -K_1 Z_1^2 - K_2 Z_2^2 \tag{24}$$

$\dot{V}_1 < 0$ is verified $\forall K_1, K_2 > 0$, therefore, the values of (23) ensure the subsystem stability in closed-loop. Assimilating (20) with (23), we obtain:

$$-K_1 Z_1 = \dot{\omega}_r^* - \frac{p^2}{J}\frac{L_m}{L_m + L_R}\varphi_r \left(i_{sq1} + i_{sq2}\right) + T_L \frac{p}{J} + \frac{K_f}{J}\omega_r \tag{25}$$

$$-K_2 Z_2 = \dot{\varphi}_r^* + \frac{R_r}{L_m + L_r}\varphi_r - \frac{R_r L_m}{L_m + L_r}\left(i_{sd1} + i_{sd2}\right) \tag{26}$$

Posing:

$$\begin{cases} i_{sd1} + i_{sd2} = i_{sd}^* \\ i_{sq1} + i_{sq2} = i_{sq}^* \end{cases} \tag{27}$$

Assuming that:

$$\begin{cases} i_{sd1}^* = i_{sd2}^* = \dfrac{i_{sd}^*}{2} \\ i_{sq1}^* = i_{sq2}^* = \dfrac{i_{sq}^*}{2} \end{cases} \tag{28}$$

Substituting (27) into (25) and (26), we obtain:

$$\begin{cases} -K_1 Z_1 = \dot{\omega}_r^* - \dfrac{p^2}{J}\dfrac{L_m}{L_m + L_r}\varphi_r i_{sq}^* + T_L \dfrac{p}{J} + \dfrac{K_f}{J}\omega_r \\ -K_2 Z_2 = \dot{\varphi}_r^* + \dfrac{R_r}{L_m + L_r}\varphi_r - \dfrac{R_r L_m}{L_m + L_r} i_{sd}^* \end{cases} \tag{29}$$

Finally, the virtual elements of control are given by:

$$i_{sq}^* = \frac{J\left(L_m + L_r\right)}{p^2 L_m \varphi_r}\left[\dot{\omega}_r^* + T_L \frac{p}{J} + \frac{K_f}{J}\omega_r + K_1 Z_1\right] \tag{30}$$

$$i_{sd}^* = \frac{L_m + L_r}{L_m R_r}\left[\dot{\varphi}_r^* + \frac{R_r}{L_m + L_r}\varphi_r + K_2 Z_2\right] \tag{31}$$

4.2 Step2: currents control (actual control)

This step establishes the control law by forcing the currents $i_{sd1}, i_{sq1}, i_{sd2}, i_{sq2}$ resulted from the first step to reach their desired references $i_{sd1}^*, i_{sq1}^*, i_{sd2}^*, i_{sq2}^*$, respectively; this objective

requires the identification of a new four errors. The tracking errors of the currents are:

$$Z_i = i_{sdi}^* - i_{sdi} \qquad i = \overline{3,6} \tag{32}$$

The derivative of (32) gives:

$$\dot{Z}_i = \frac{d}{dt} i_{sdi}^* - \frac{d}{dt} i_{sdi} \qquad i = \overline{3,6} \tag{33}$$

Substituting the derivatives of currents from (1) into (33), we obtain:

$$\dot{Z}_3 = \frac{d}{dt} i_{sd1}^* - \frac{1}{L_{s1}} \left[v_{sd1} - R_{s1} i_{sd1} + \omega_s \left(L_{s1} i_{sq1} + T_r \varphi_r \omega_{gl} \right) \right] \tag{34}$$

$$\dot{Z}_4 = \frac{d}{dt} i_{sd2}^* - \frac{1}{L_{s2}} \left[v_{sd2} - R_{s2} i_{sd2} + \omega_s \left(L_{s2} i_{sq2} + T_r \varphi_r \omega_{gl} \right) \right] \tag{35}$$

$$\dot{Z}_5 = \frac{d}{dt} i_{sq1}^* - \frac{1}{L_{s1}} \left[v_{sq1} - R_{s1} i_{sq1} - \omega_s \left(L_{s1} i_{sd1} + \varphi_r \right) \right] \tag{36}$$

$$\dot{Z}_6 = \frac{d}{dt} i_{sq2}^* - \frac{1}{L_{s2}} \left[v_{sq2} - R_{s2} i_{sq2} - \omega_s \left(L_{s2} i_{sd2} + \varphi_r \right) \right] \tag{37}$$

We notice that the actual control variables v_{sd1}, v_{sd2}, v_{sq1}, v_{sq2} appeared in (34)-(37), therefore the increased Lyapunov function V_2 is defined by:

$$V_2 = \frac{1}{2} \left(Z_1^2 + Z_2^2 + Z_3^2 + Z_4^2 + Z_5^2 + Z_6^2 \right) \tag{38}$$

We take note that V_2 is chosen in such a way that permits achieving control law .The corresponding time derivative of the positive definite function V_2 is:

$$\dot{V}_2 = -K_1 Z_1^2 - K_2 Z_2^2 + Z_3 \dot{Z}_3 + Z_4 \dot{Z}_4 + Z_5 \dot{Z}_5 + Z_6 \dot{Z}_6 \tag{39}$$

By applying the Lyapunov stability theorem as in the first step, we choose:

$$\dot{Z}_i = -K_i Z_i \qquad i = \overline{3,6} \tag{40}$$

The derivative of the global Lyapunov function is negative definite. Finally, putting the equivalence between (33) and (40), we find the real control represented by the following equations:

$$v_{sd1} = L_{s1} \frac{d}{dt} i_{sd1}^* + R_{s1} i_{sd1} - \omega_s \left(L_{s1} i_{sq1} + T_L \varphi_r \omega_{gl} \right) + K_3 Z_3 \tag{41}$$

$$v_{sd2} = L_{s2} \frac{d}{dt} i_{sd2}^* + R_{s2} i_{sd2} - \omega_s \left(L_{s2} i_{sq2} + T_L \varphi_r \omega_{gl} \right) + K_4 Z_4 \tag{42}$$

$$v_{sq1} = L_{s1} \frac{d}{dt} i_{sq1}^* + R_{s1} i_{sq1} + \omega_s \left(L_{s1} i_{sd1} + \varphi_r \right) + K_5 Z_5 \tag{43}$$

$$v_{sq2} = L_{s2} \frac{d}{dt} i_{sq2}^* + R_{s2} i_{sq2} + \omega_s \left(L_{s2} i_{sd2} + \varphi_r \right) + K_6 Z_6 \tag{44}$$

The overall scheme of the Backstepping control is represented in Fig. 1.

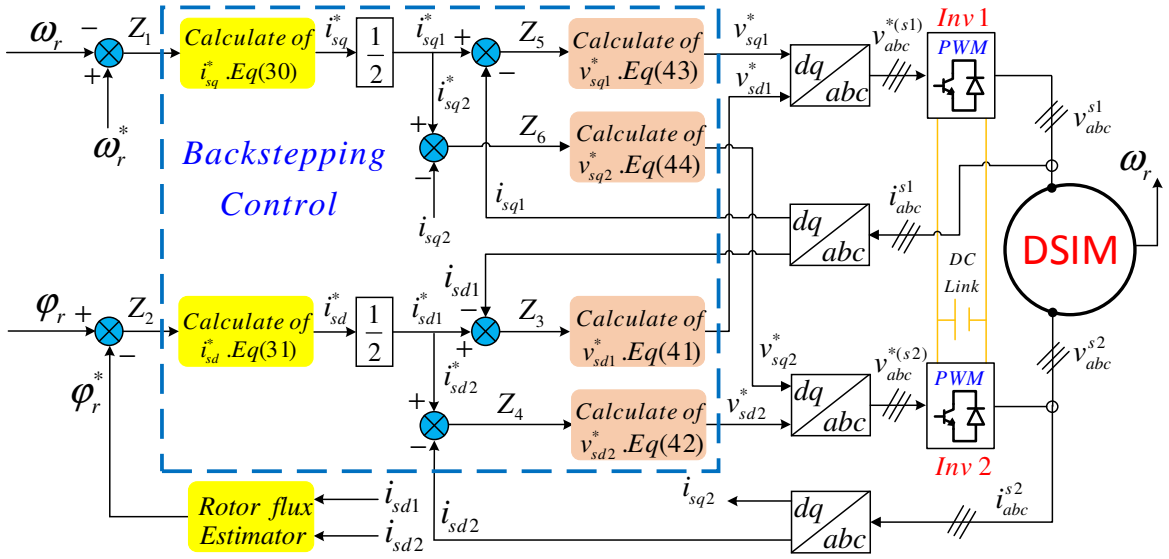

Figure 1 Backstepping control design

5. SIMULATION RESULTS AND INTERPRETATION

The DSWIM studied in this paper is powered by two voltage source inverters with a pulse width modulation (PWM) control strategy. Its nominal electrical and mechanical parameters are given in table 1. Throughout the simulation, the value of the reference flux is maintained at 1Wb thanks to a weakening block.

5.1 Healthy case

The reference speed is fixed at +300 rd/s and -300 rd/s in speed reversal mode. The DSWIM is only under the load torque (equal to the nominal value 15N.m) which is applied at t=1sec, followed by a reversal of speed at t=1.5sec. Fig. 2 shows the performance of the SMC and BSC in various operating modes of the DSWIM, such as: start-up, load application and reverse speed. Fig. 2.a shows the speed responses for both control methods, in both signals, the speed follows its reference value with a negligible overtake and without oscillations, but it clearly shows that the BSC has a faster response than the SMC and imposes a short transient regime with a response time equals 0.35sec, while for SMC, the response time is 0.36sec. No ripples in electromagnetic signals, as illustrated in Fig. 2.b proving that both control schemes are able to surmount the external load torque rejection. At start-up, the electromagnetic torque presents oscillations and a peak of 107N.m, 65N.m for SMC and BSC, respectively. At speed reversal, the electromagnetic torque decreased to 59N.m with both controls, but the BSC has the fastest dynamic response. After each transient regime, the electromagnetic torque compensates the friction losses and the load torque. Fig. 2.c shows that BSC and SMC are suitable to lead the flux to it desired reference (1Wb), BSC also has the fastest dynamic response than SMC, which represents ripples at startup. Finally Fig. 2.d shows the behavior of the line current i_{sa1} of the first stator. For both control techniques, the current shape is sinusoidal, slightly affected by the switching frequency generated by the inverter. During the dynamic state (at start-up and speed reversal), the DSWIM consumes very important current but does not exceed the nominal value, when inserting the load, the amplitude of currents reaches 6.5A. The obtained results in a healthy state summarize and reflect a slight superiority in the response swiftness of the BSC over the SMC.

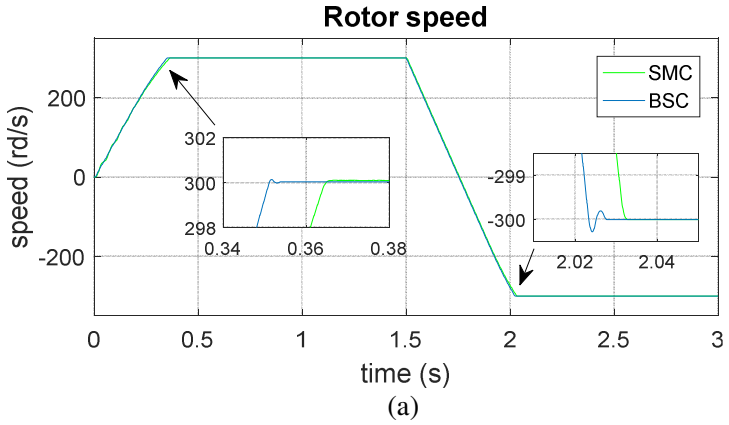

(a)

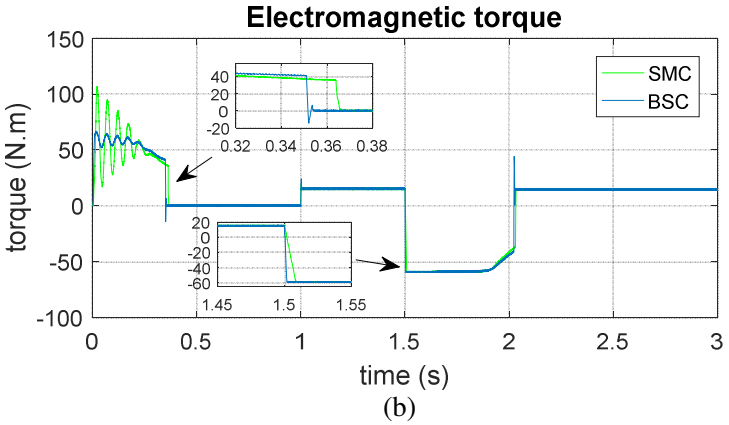

(b)

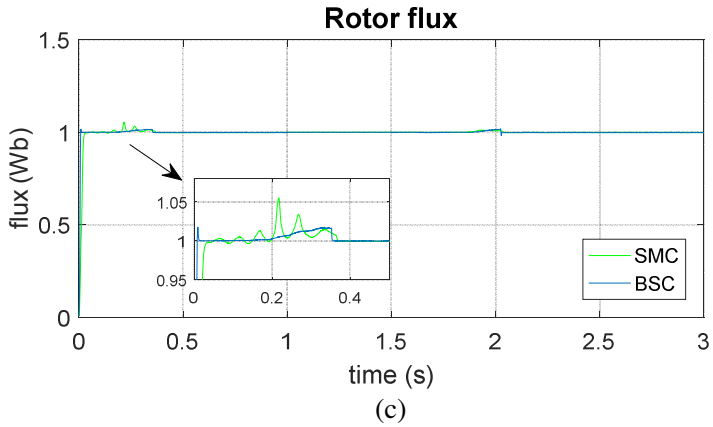

(c)

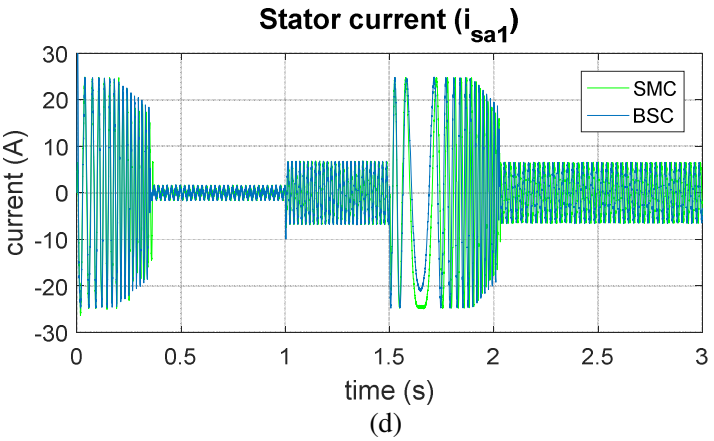

(d)

Figure 2 Simulation results of SMC and BSC

TABLE I. MACHINE PARAMETERS [9]

Identifiers & values	Parameters
Rs1 = 3.72 Ω	Stator1 resistance
Rs2 = 3.72 Ω	Stator2 resistance
Rr = 2.12 Ω	Rotor resistance
Ls1 = 0.022 H	Stator1 inductance
Ls2 = 0.022 H	Stator2 inductance
Lr = 0.006 H	Rotor inductance
Lm = 0.3672 H	Mutuel inductance
J = 0. 0625 Kgm^2	Inertia
Kf = 0.001 $Nm.(rd/s)^{-1}$	damping coefficient
p = 1	Number of pole pairs

5.2 Parametric variation case

In order to prove the effectiveness and robustness of the sliding mode control and backstepping control for the dual stator winding induction machine, disturbance of 10% of the nominal value is introduced into the inductance parameter (increasing of 10% in L_{s1}). The simulations presented in Fig. 3 illustrate the performance of the two control schemes under this abnormal condition, we clearly notice from speed and flux signals (Fig. 3.a and Fig. 3.c) that the BSC ensures a better robustness against parameter variation even with a load torque, at t=1.5sec, a peak of 36 N.m appears in the signals of electromagnetic torque as shown in Fig. 3.b. The amplitude of stator phase currents decreases to 4A as illustrated in Fig. 3.d. In order to confirm the superiority of the BSC algorithm over that of SMC, different indicators are reported in table 2: peak overshoot, integral absolute error (IAE), integral of square error (ISE) and integral time absolute error (ITAE) [8].

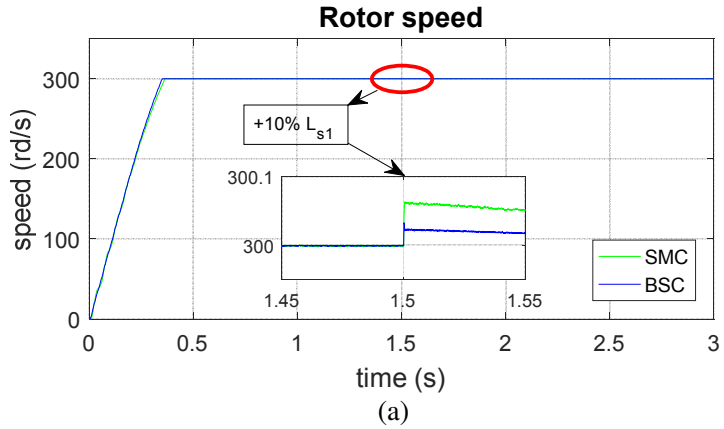

(a)

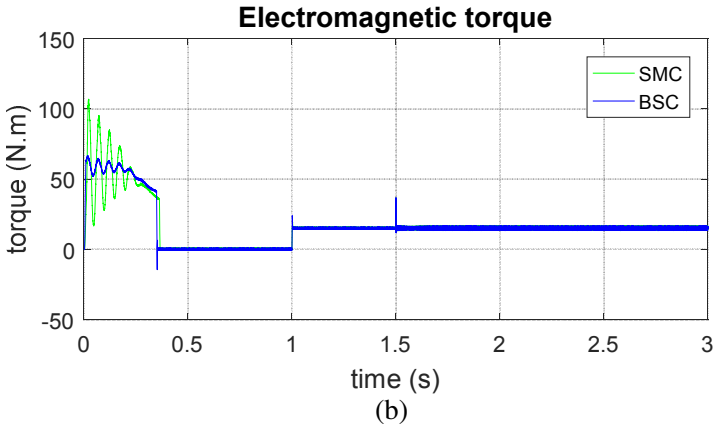

(b)

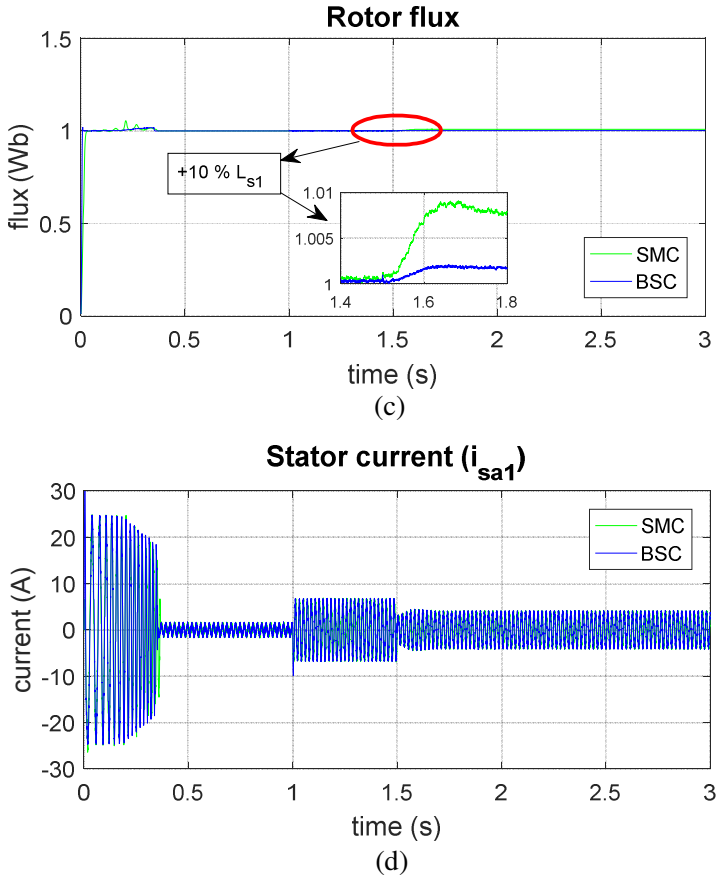

Figure 3 DSWIM performances with SMC and BSC (+ 10% L_{s1}at t=1.5 s).

TABLE II. PERFORMANCE INDICATORS

Control strategy	Peak overshoot (%)	$IAE = \int \lvert e \rvert dt$
SMC	0.0467	0.07506
BSC	0.0333	0.02645
Control strategy	$ISE = \int \lvert e \rvert^2 dt$	$ITAE = \int t \lvert e \rvert dt$
SMC	0.0037	0.168
BSC	0.0004657	0.05885

6. CONCLUSIONS

In this paper, a comparative study between the backstepping control and the sliding mode control for a dual stator winding induction machine is carried out. Simulation results showed the robustness of the two control methods during the healthy operation and also under parametric variation, concluding that the speed and flux references are kept after the increase of the inductive parameter with a good tracking and without oscillations in the electromagnetic torque with a total rejection of the load torque disturbance. The steady state stability performance indicators show a slight superiority of the BSC over the SMC, but this small difference can be fatal for the SMC when the machine is in a fault condition, as all errors will be multiplied. As future work, the backstepping control will be associated with an active fault-tolerant control system with a sensorless version.

REFERENCES

[1] N. Layadi, S. Zeghlache, T. Benslimane and F. Berrabah, "Comparative Analysis between the Rotor Flux Oriented Control and Backstepping Control of a Double Star Induction Machine (DSIM) under Open-Phase Fault," AMSE Journals, Series Advances C, Vol. 72, No.4, pp. 292-311, 2017.

[2] L. Youb, S. Belkacem, F. Naceri, M. Cernat, and L. G. Pesquer, "Design of an Adaptive Fuzzy Control System for Dual Star Induction Motor Drives," Advances in Electrical and Computer Engineering, Vol. 18, No.3, pp. 37-44, 2018.

[3] Y. Yang, and Y. Yan, "Backstepping sliding mode control for uncertain strict-feedback nonlinear systems using neural-network-based adaptive gain scheduling," Journal of Systems Engineering and Electronics, Vol. 29, No.3, pp. 580-586, 2018.

[4] M. El Azzaoui, H. Mahmoudi, B. Bossoufi, and M. El Ghamrasni, "Comparative study of the sliding mode and backstepping control in power control of a doubly fed induction generator," Proceedings of the International Symposium on Fundamentals of Electrical Engineering, Bucharest, Romania, pp.1-5, 2016.

[5] J. Listwan, and K. Pieńkowski, "Sliding-mode direct field-oriented control of six-phase induction motor," Technical Transactions, Vol. (2-E), pp. 95-108, 2016.

[6] H. Amimeur, R. Abdessemed, D. Aouzellag, K. Ghedamsi, F. Hamoudi, and S. Chekkal, "A sliding mode control for dual-stator induction motor drives fed by matrix converters," J Eletric Eng, Vol. 11, No.2, pp.136-143, 2011.

[7] N. Djeghali, M. Ghanes, S. Djennoune, and J. P. Barbot, "Sensorless fault tolerant control for induction motors," International Journal of Control, Automation and Systems, Vol. 11, No.3, pp. 563-576, 2013.

[8] A. Djerioui, A. Houari, M. Ait-Ahmed, M. F. Benkhoris, A. Chouder, and M. Machmoum, "Grey Wolf based control for speed ripple reduction at low speed operation of PMSM drives," ISA transactions, Vol. 74, pp. 111-119, 2018.

[9] S. Lekhchine, T. Bahi, and Y. Soufi, "Indirect rotor field oriented control based on fuzzy logic controlled double star induction machine," International Journal of Electrical Power & Energy Systems, Vol. 57, pp. 206-211, 2014.